



Title	Selective hydrogenation of chloronitrobenzene to chloroaniline in supercritical carbon dioxide over Ni/TiO <sub>2</sub> : Significance of molecular interactions
Author(s)	Meng, Xiangchun; Cheng, Haiyang; Fujita, Shin-ichiro et al.
Citation	Journal of Catalysis, 269(1), 131-139 <a href="https://doi.org/10.1016/j.jcat.2009.10.024">https://doi.org/10.1016/j.jcat.2009.10.024</a>
Issue Date	2010-01-01
Doc URL	<a href="https://hdl.handle.net/2115/42642">https://hdl.handle.net/2115/42642</a>
Type	journal article
File Information	JC269-1_131-139.pdf



**Selective hydrogenation of chloronitrobenzene to chloroaniline in  
supercritical carbon dioxide over Ni/TiO<sub>2</sub>: Significance of molecular  
interactions**

Xiangchun Meng<sup>a,b,c</sup>, Haiyang Cheng<sup>b</sup>, Shin-ichiro Fujita<sup>a</sup>, Yufen Hao<sup>b</sup>, Yanjiao Shang<sup>b</sup>,

Yancun Yu<sup>b</sup>, Shuxia Cai<sup>b</sup>, Fengyu Zhao<sup>b,\*</sup>, Masahiko Arai<sup>a,\*</sup>

<sup>a</sup> *Division of Chemical Process Engineering, Graduate School of Engineering,*

*Hokkaido University, Sapporo 060-8628, Japan.*

Tel & Fax: +81 11 706 6594.

E-mail: marai@eng.hokudai.ac.jp (M. Arai).

<sup>b</sup> *State Key Laboratory of Electroanalytical Chemistry, Changchun Institute of Applied*

*Chemistry, Chinese Academy of Sciences, Changchun 130022, China.*

Tel: +86 431 8526 2410; Fax: +86 431 8526 2410.

E-mail: zhaofy@ciac.jl.cn (F. Zhao)

<sup>c</sup> *School of Chemical Engineering, Changchun University of Technology, Changchun*

*130012, China.*

## Abstract

The hydrogenation of chloronitrobenzene to chloroaniline was investigated over Ni/TiO<sub>2</sub> at 35°C in supercritical CO<sub>2</sub> (scCO<sub>2</sub>), ethanol, and *n*-hexane. The reaction rate followed the order of scCO<sub>2</sub> > *n*-hexane > ethanol. In scCO<sub>2</sub>, the selectivity to chloroaniline and to aniline over Ni/TiO<sub>2</sub> were 97–99.5% and <1%, respectively, in the conversion range of 9–100%. The high chemoselectivity to chloroaniline cannot be achieved over Ni/TiO<sub>2</sub> in ethanol and *n*-hexane. *In situ* high-pressure Fourier transform infrared measurements were made to study the molecular interactions of CO<sub>2</sub> with the following reactant and reaction intermediates: chloronitrobenzene, chloronitrosobenzene, and *N*-chlorophenylhydroxylamine. The molecular interaction modifies the reactivity of each species and accordingly the reaction rate and the selectivity. The influence of Cl substituent on the interaction modes of CO<sub>2</sub> with these reacting species is discussed. Possible reaction pathways for the hydrogenation of chloronitrobenzene in scCO<sub>2</sub> over Ni/TiO<sub>2</sub> are also proposed.

**Keywords:** Chloronitrobenzene, Chloroaniline, Hydrogenation, Carbon dioxide, Intermolecular interaction

## 1. Introduction

The catalytic hydrogenation of chloronitrobenzene (CNB) is a common method to manufacture chloroaniline (CAN) isomers (*o*-, *m*-, and *p*-CAN), which are important intermediates in the synthesis of dyes, pharmaceuticals, and agricultural chemicals [1]. The hydrogenation of CNB, depending on the catalyst used, yields CAN through several possible pathways along with some reaction intermediates such as chloronitrosobenzene (CNSB), *N*-chlorophenylhydroxylamine (CPHA), dichloroazoxybenzene (CAOB), dichloroazobenzene (CAB), and dichlorohydrazobenzene (CHAB) (Scheme 1) [2-5]. The accumulation of these intermediates, especially CPHA, is critical when the hydrogenation of CNB is carried out in batch reactors at low or medium temperatures [3]. Because these compounds are highly toxic and problematic, their accumulation during the reaction should be avoided for the safe and green production of CAN [3-5]. To avoid the accumulation of CPHA, it is of advantage to carry out the hydrogenation at temperatures  $>80^{\circ}\text{C}$  over well-designed catalysts [4]. Chemoselective hydrogenation of aromatic nitro compounds was achieved over Au/TiO<sub>2</sub> and Au/Fe<sub>2</sub>O<sub>3</sub> at 100–130°C, with only trace amounts of intermediates formed [6]. The addition of small amounts of vanadium promoters could reduce the accumulation of arylhydroxylamine during the

hydrogenation (120°C) of aromatic nitro compounds over commercial Pd and Pt catalysts [3]. For Raney Ni catalysts used for the hydrogenation (30–35°C) in organic solvents, however, the selection of effective promoters is difficult because modifiers that reduce the accumulation usually lower the reaction rate [7]. Mahata et al. communicated that when the hydrogenation of CNB was performed at 120°C over filamentous carbon stabilized Ni catalyst in methanol, the specific activity was ~50 mmol h<sup>-1</sup> g<sup>-1</sup> Ni (2.9 mmol h<sup>-1</sup> mmol<sup>-1</sup> Ni) and there was no intermediate detected at any level of CNB conversion [8]. Their catalyst was prepared by methane decomposition over Raney Ni, which is expensive for industrial catalyst preparation. Keane and coworkers reported that selective production of CAN could be achieved in the gas phase hydrogenation of CNB over Au/Al<sub>2</sub>O<sub>3</sub> (120–250°C), Pd-promoted Au/Al<sub>2</sub>O<sub>3</sub> (Au/Pd mol/mol ≥ 20) (120°C), and supported Ni catalysts (120°C) [5, 9].

Dechlorination of CAN to aniline (AN) or of CNB to nitrobenzene (steps VIII, IX in Scheme 1) is another side reaction that decreases the selectivity to CAN and results in the formation of hydrogen chloride. Addition of inhibitors can minimize dechlorination, but usually lowers the reaction rate. It has recently been reported that the dechlorination process can almost completely be suppressed over several novel catalysts such as Ag/SiO<sub>2</sub> [10], Au/SiO<sub>2</sub> [11], Au/ZrO<sub>2</sub> [12], AuPd/Al<sub>2</sub>O<sub>3</sub> [9], Au/Fe(OH)<sub>x</sub> [13],

Pt/ $\gamma$ -Fe<sub>2</sub>O<sub>3</sub> [14, 15], Pt/ $\gamma$ -ZrP [16], decorated Pt/TiO<sub>2</sub> [17, 18], Ru/SnO<sub>2</sub> [1], and Ni/TiO<sub>2</sub> [19]. The hydrogenation was usually carried out at 90–150°C with Au and Ag [9-13], at 75–120°C with Ni [8, 19], and at 30–60°C over Pt catalysts [14-18]. With these catalysts, the selectivity to the undesired AN was <1% at complete conversion of CNB. However, the use of these noble metal catalysts (Au, Ag, Pd, Ru, and Pt) in large-scale production should be practiced after a prudential consideration of the cost. Additionally, it seems necessary to improve the activity of Au and Ag catalysts for practical applications [15]. With Pt/Fe<sub>2</sub>O<sub>3</sub>, Pt/ $\gamma$ -ZrP, and Ni/TiO<sub>2</sub>, harmful reaction intermediates such as CNSB, CPHA, CAOB, and CAB were formed in organic solvents during the reaction [14-16, 19].

The melting point of *o*-, *m*-, and *p*-CNB is 32.1, 44.4, and 82°C, respectively. To dissolve the solid CNB substrates (at room temperature), organic solvents such as methanol, ethanol, 1-butanol, hexane, cyclohexane, ethyl acetate, diethyl ether, and tetrahydrofuran are frequently used in both the liquid and the conventional gas phase hydrogenation [1-19]. These organic solvents are volatile, toxic, and associated with serious health hazards and environmental problems. The use of traditional organic solvents is considered a major source of waste in the chemical industry. Thus, removal of the toxic solvents is significant to achieve the green production of CAN. Ionic liquid

was used as a medium for the hydrogenation of *o*-CNB over ionic-liquid-like copolymer stabilized Pt nanocatalysts, and the selectivity to CAN was >96% [20]. Because toxic organic solvents are generally used in the synthesis of ionic liquids, supercritical carbon dioxide (scCO<sub>2</sub>) might be a greener alternative to conventional organic solvents. ScCO<sub>2</sub> has several merits such as nonflammability, relative inertness, complete miscibility with gases, and easy separation from liquid/solid products after reactions [21-27].

Furthermore, scCO<sub>2</sub> can show interesting effects on reaction rate and product selectivity [28-32]. Ichikawa et al. reported that the rate of hydrogenation of CNB over Pt/C was markedly enhanced and the dechlorination reaction was significantly suppressed in scCO<sub>2</sub>. The selectivity to CAN was >99% at 100% conversion; however, they did not mention whether there were intermediates accumulated during the course of reaction to the complete conversion [32]. The present authors previously showed that undesired intermediates were formed and accumulated during the hydrogenation of nitrobenzene on Pt/C in scCO<sub>2</sub> [33, 34]. With Pd/C, the selectivity to *o*-CAN in scCO<sub>2</sub> (92–94%) was also higher than that in ethanol (84%), but it is difficult to suppress the dechlorination reaction completely [35]. In our attempts to use supported Au catalysts such as Au/TiO<sub>2</sub> and Au/SiO<sub>2</sub> in scCO<sub>2</sub> for the CNB hydrogenation, the activity of Au catalysts was lowered monotonously with the addition of CO<sub>2</sub>. The reduction of Au activity in dense

phase CO<sub>2</sub> was possibly due to the interaction of CO<sub>2</sub> with Au [36]. As to Pt/ $\gamma$ -Fe<sub>2</sub>O<sub>3</sub> and Au/Fe(OH)<sub>x</sub>, the acid formed in situ from CO<sub>2</sub> and a hydrogenation byproduct of H<sub>2</sub>O are likely to impose negative effects on the support Fe<sub>2</sub>O<sub>3</sub> or Fe(OH)<sub>x</sub>.

Thus, it remains to be a challenging task to achieve a high chemoselectivity to CAN for the hydrogenation of CNB in green solvents over non-noble metal catalysts. Recently we have shown that the selective hydrogenation of nitrobenzene can be achieved over Ni/ $\gamma$ -Al<sub>2</sub>O<sub>3</sub> in dense phase CO<sub>2</sub> with 99% selectivity to AN over the whole conversion range of 0-100%, and molecular interactions of CO<sub>2</sub> with the reaction species are significant for the improvement in the selectivity [37]. The hydrogenation of CNB has a stronger tendency to give arylhydroxylamine in large amounts during the reaction [3]. Therefore, it is interesting and significant to see whether the dechlorination reaction and the accumulation of intermediates can be suppressed simultaneously during the hydrogenation of CNB with the Ni-scCO<sub>2</sub> system. The molecular interaction of CO<sub>2</sub> with CNB, CNSB, and CPHA is also a question of common interest because there is an electron-withdrawing substituent, -Cl, attaching to the benzene ring of CNB, CNSB, and CPHA. In this work, we have studied the hydrogenation of *o*-, *m*-, and *p*-CNB over Ni/ $\gamma$ -Al<sub>2</sub>O<sub>3</sub> and Ni/TiO<sub>2</sub> in scCO<sub>2</sub> at 35°C. For comparison, the hydrogenation was also examined in ethanol and *n*-hexane under similar reaction conditions. *In situ*

high-pressure Fourier transform infrared (FTIR) measurements were made to study the molecular interactions of dense phase CO<sub>2</sub> with CNB, CNSB, and CPHA molecules.

## **2. Experimental**

### **2.1. Catalyst preparation and characterization**

Ni/TiO<sub>2</sub> was prepared by incipient wetness impregnation using anatase TiO<sub>2</sub> (specific surface area 120 m<sup>2</sup> g<sup>-1</sup>, Nanjing High Technology Nano Material Co., Ltd., China) and Ni(NO<sub>3</sub>)<sub>2</sub>·6H<sub>2</sub>O. Ni/Al<sub>2</sub>O<sub>3</sub> was prepared by co-precipitation using Ni(NO<sub>3</sub>)<sub>2</sub>·6H<sub>2</sub>O and Al(NO<sub>3</sub>)<sub>3</sub> with a Ni/Al atomic ratio of 1/1 [37]. After drying at 120°C, the two catalysts were calcined at 450°C for 5 h. Before the hydrogenation run, the calcined samples were reduced under H<sub>2</sub> flow at 450 and 610°C for Ni/TiO<sub>2</sub> and Ni/Al<sub>2</sub>O<sub>3</sub>, respectively.

The Ni loading in the calcined samples of Ni/Al<sub>2</sub>O<sub>3</sub> and Ni/TiO<sub>2</sub> was measured by inductively coupled plasma optical emission spectrometry. The structural properties of Ni catalysts were examined by X-ray diffraction (XRD, Philips PW1710 BASED) and transmission electron microscopy (TEM, JEM-2000EX).

### **2.2. CNB hydrogenation**

The hydrogenation of CNB was examined over both catalysts at 35°C. The reaction runs in scCO<sub>2</sub> were conducted in a 50 cm<sup>3</sup> autoclave. The reactor was charged

with CNB 1.5 g (9.52 mmol) and a catalyst sample (0.15 g Ni/TiO<sub>2</sub> or 0.1 g Ni/Al<sub>2</sub>O<sub>3</sub>), flushed with N<sub>2</sub>, and placed into a water bath preset to 35°C for 20 min. After the introduction of 4 MPa H<sub>2</sub>, liquid CO<sub>2</sub> was introduced into the reactor with a high-pressure liquid pump (Jasco SCF-Get) to the desired pressure. The reaction was conducted while the reaction mixture was being stirred with a magnetic stirrer. After the reaction, the reactor was cooled with an ice-water bath for 20 min, depressurized carefully, and the reaction mixture was analyzed with a gas chromatograph (Shimadzu GC-2010, Rtx-5 capillary column) using a flame ionization detector. Hydrogenation reactions in ethanol and *n*-hexane were conducted in the same reactor using similar procedures. To ensure the amount of hydrogen in the reactor is enough for a complete conversion of CNB, all reactions were performed at an initial H<sub>2</sub> pressure of 4 MPa; the hydrogenation could proceed smoothly at lower H<sub>2</sub> pressures, as shown in our previous work [37].

### **2.3. Phase behavior and FTIR measurements**

The solubility of CNB in scCO<sub>2</sub> in the presence of 4 MPa H<sub>2</sub> was measured at 35°C by the naked eye through the transparent sapphire windows attached to an 85 cm<sup>3</sup> high-pressure reactor. Different amounts of CNB substrate were added into the reactor and the CO<sub>2</sub> pressures corresponding to phase transition were carefully determined. The

details of experimental procedures were described elsewhere [31]. The phase behavior of the reactant mixture (i.e., H<sub>2</sub> and CNB) in dense phase CO<sub>2</sub> was also examined in the same reactor; the observation was made with a similar mass/volume ratio of CNB to the reactor volume as used in the hydrogenation runs.

The high-pressure FTIR was used to examine the molecular interactions of CO<sub>2</sub> with reacting species. The FTIR spectra of *p*-CNB, *p*-CNSB, and *p*-CPHA in dense phase CO<sub>2</sub> were collected with the same spectrometer in similar fashions as used in the previous work [31]. The measurements were made at 35°C and in the presence of 0–20 MPa CO<sub>2</sub> and 4 MPa H<sub>2</sub>. The weight of samples used was changed depending on its solubility in CO<sub>2</sub>. A higher temperature of 90°C was also used for *p*-CNB and *p*-CNSB at CO<sub>2</sub> pressures < 4 MPa and < 6 MPa, respectively. For those measurements, *p*-CNB (Wako) was used as received; commercially unavailable *p*-CNSB and *p*-CPHA, two of the intermediates (Scheme 1), were synthesized by the oxidation of *p*-CAN (Wako) with H<sub>2</sub>O<sub>2</sub> catalyzed with ammonium molybdate [38], and by the reduction of *p*-CNB with zinc dust [39], respectively. The formation of these compounds was confirmed by FTIR and NMR (JEOL A200II) [38, 40].

### **3. Results and discussion**

#### **3.1. Properties of Ni catalysts**

Ni/Al<sub>2</sub>O<sub>3</sub> was the same as used previously for the hydrogenation of nitrobenzene; the average Ni particle size was ca. 8.5 nm [37]. The Ni loading of Ni/Al<sub>2</sub>O<sub>3</sub> and Ni/TiO<sub>2</sub> was 41% and 16%, respectively. The XRD patterns and TEM images of Ni/TiO<sub>2</sub> are presented in Fig. 1. After calcination, the existence of NiO and anatase TiO<sub>2</sub> was identified. After reduction, Ni particles in size mostly between 5–25 nm were formed. The average particle size determined from the XRD line broadening was ca. 14 nm.

### **3.2. Features of Ni catalysts for selective hydrogenation of CNB**

Table 1 shows the results of *o*-CNB hydrogenation over Ni/Al<sub>2</sub>O<sub>3</sub> and Ni/TiO<sub>2</sub> in scCO<sub>2</sub> at 35°C. The selectivity to the desired *o*-CAN at ca. 80% conversion was > 98% and 99% over Ni/Al<sub>2</sub>O<sub>3</sub> and Ni/TiO<sub>2</sub>, respectively. Moreover, the turnover frequency (TOF) value for the reaction over Ni/Al<sub>2</sub>O<sub>3</sub> was much less than that over Ni/TiO<sub>2</sub> (entries 1, 2). These results indicate that chemoselective hydrogenation of *o*-CNB can be achieved in scCO<sub>2</sub> over both Ni catalysts, especially over Ni/TiO<sub>2</sub>.

Table 1 also compares the results of *o*-CNB hydrogenation over Ni/TiO<sub>2</sub> in scCO<sub>2</sub> with that in polar ethanol and apolar *n*-hexane at 35°C. The rate of *o*-CNB conversion was the highest in scCO<sub>2</sub> and the lowest in ethanol. The TOF value in scCO<sub>2</sub> was ~3.1 and ~1.4 times higher than that in ethanol and *n*-hexane, respectively. In ethanol, the

dechlorination reaction was negligible but the intermediates including CNSB, CAO, CAB, and CHAB were formed in a significant amount (entries 3, 4). Because CPHA decomposes to CNSB and CAN during gas chromatograph analysis [42], the formation of CPHA during the hydrogenation cannot be excluded. Chen and coworkers, who performed the hydrogenation of CNB at 90°C over Ni/TiO<sub>2</sub> in ethanol, also observed the formation of significant amounts of intermediates and negligible amount of AN [19]. In contrast, there was no accumulation of intermediates in *n*-hexane, but a slight dechlorination occurred (entry 5). In scCO<sub>2</sub>, both of the dechlorination and the accumulation of intermediates were suppressed satisfactorily; the selectivity to *o*-CAN was 99% at 82% conversion (entry 2).

Fig. 2 shows the evolution of product species with time during the hydrogenation of *o*-CNB over Ni/TiO<sub>2</sub> in scCO<sub>2</sub>. The yield of *o*-CAN is similar to the conversion of *o*-CNB over the whole conversion range from 9 to ~100%; the yield of all byproducts including AN and reaction intermediates decreased from < 3.5% in 5 min to < 1% after 30 min. Thus, Ni/TiO<sub>2</sub> is very effective for the chemoselective hydrogenation of *o*-CNB in scCO<sub>2</sub>. The combination of scCO<sub>2</sub> and Ni/TiO<sub>2</sub> is also effective for the chemoselective hydrogenation of *m*- and *p*-CNB isomers (Table 2).

The suppression of formation of hydroxylamine is a topic of industrial importance

because aryl hydroxylamines are generally accumulated in large amounts during the hydrogenation of nitroaromatics with electron-withdrawing substituents (e.g., halogen or sulfonamide) [3, 7]. Studer et al. found that the accumulation of hydroxylamine in methanol at 30–35°C could be reduced from 70–80% over unmodified Raney Ni to 11% by careful selection of vanadium promoters; simultaneously, the reaction rate was down by a factor of 0.1 [7]. Mahata et al. communicated that there was no intermediate detected in methanol during the hydrogenation of *o*- and *p*-CNB over filamentous carbon stabilized Ni catalyst, and the specific activity was  $\sim 50 \text{ mmol h}^{-1} \text{ g}^{-1} \text{ Ni}$  ( $2.9 \text{ mmol h}^{-1} \text{ mmol}^{-1} \text{ Ni}$ ) at 120°C under 1.5 MPa H<sub>2</sub> [8]. Recently, we have shown that the accumulation of intermediates during the hydrogenation of nitrobenzene can be completely avoided over Ni/Al<sub>2</sub>O<sub>3</sub> in dense phase CO<sub>2</sub> [37]. The present hydrogenation of *o*-CNB over Ni/TiO<sub>2</sub> in scCO<sub>2</sub> gave a TOF value of 318 h<sup>-1</sup> ( $22.9 \text{ mmol h}^{-1} \text{ mmol}^{-1} \text{ Ni}$ ) at 35°C under an initial H<sub>2</sub> pressure of 4 MPa; the TOF value was much higher than that in ethanol and *n*-hexane (Table 1). Additionally, it is difficult to achieve a high chemoselectivity in both ethanol and *n*-hexane because either significant accumulation of intermediates or slight dechlorination takes place. In the context, the present results are important because the reduction of intermediates can be achieved along with the increased reaction rate and the negligible dechlorination. In other words, the

effectiveness of scCO<sub>2</sub> and Ni catalysts for the reduction of intermediates can be extended to a more challenging task of chemoselective hydrogenation of CNB in the absence of organic solvents. To our knowledge, such a chemoselective hydrogenation of CNB to CAN over Ni catalysts at mild temperature has not been reported so far.

### 3.3. Influence of CO<sub>2</sub> pressure and phase behavior

The present hydrogenation occurs in a multi-phase system, in which the reaction rate and/or the product distribution may depend on the phase behavior. The hydrogenation of CNB was studied with the most effective Ni/TiO<sub>2</sub> catalyst at different CO<sub>2</sub> pressures while making the other conditions unchanged. Before the reaction results, the phase behavior observations are given first. Fig. 3 shows the changes in the phase state of CNB isomers in scCO<sub>2</sub> at different CO<sub>2</sub> pressures and at 35°C in the presence of 4 MPa H<sub>2</sub>. At 35°C, *m*- and *p*-CNB are solid in the absence of CO<sub>2</sub>; *m*-CNB turned into liquid at ca. 3.6 MPa CO<sub>2</sub>, indicating that its melting point could be lowered to < 35°C under dense phase CO<sub>2</sub>. The CNB substrates were soluble to some extent in scCO<sub>2</sub> at 35°C and their quantities in scCO<sub>2</sub> increased with CO<sub>2</sub> pressure. The solubility was influenced somewhat by the substituent position of the CNB isomers and followed the order of *m*- > *o*- and *p*-CNB. With the same ratio of CNB weight to reactor volume as used in the hydrogenation runs, the phase transition from two phases to a single one

occurred at CO<sub>2</sub> pressures of 12.3, 10.2, and 12.8 MPa for *o*-, *m*-, and *p*-CNB, respectively. Upon careful depressurization, the reverse transition was observed at 11.8, 9.6, and 11.6 MPa for *o*-, *m*-, and *p*-CNB, respectively.

The influence of CO<sub>2</sub> pressure was examined with a selected substrate of *o*-CNB. Fig. 4 shows the changes in the conversion of *o*-CNB and the selectivity to *o*-CAN with CO<sub>2</sub> pressure. The total conversion of *o*-CNB increased first and then decreased with increasing CO<sub>2</sub> pressure. The conversion was maximal at ca. 9–12.5 MPa CO<sub>2</sub>. The pressure for the maximum conversion is close to that of the reversible phase transition of *o*-CNB (11.8–12.3 MPa CO<sub>2</sub>), indicating that the phase behavior is an important factor in determining the rate of CNB hydrogenation. However, the high selectivity to *o*-CAN remained unchanged when the reaction mixture changed from the gas–liquid–solid system to the gas–solid one.

### **3.4. FTIR measurements: molecular interactions with CO<sub>2</sub>**

High-pressure FTIR was used to examine molecular interactions of dense phase CO<sub>2</sub> with such selected reacting species as *p*-CNB, *p*-CNSB, and *p*-CPHA, which would affect the reaction pathways of selective hydrogenation of CNB and change the reaction rate and the product selectivity.

#### **3.4.1 *p*-CNB**

Fig. 5 shows the FTIR spectra of nitro group vibrations in the presence of 4 MPa H<sub>2</sub> and 0–20 MPa CO<sub>2</sub>. The result of *p*-CNB in ethanol is also shown for comparison. The bands at ca. 1343 and 1521 cm<sup>-1</sup> were assigned to the symmetric and asymmetric stretching vibrations of the nitro group,  $\nu_s(\text{NO}_2)$  and  $\nu_{as}(\text{NO}_2)$  [2]. The peaks of  $\nu_s(\text{NO}_2)$  and  $\nu_{as}(\text{NO}_2)$  were shifted with CO<sub>2</sub> pressure, and these shifts are depicted in Fig. 6. The peak position of  $\nu_s(\text{NO}_2)$  was blue shifted from 1343 cm<sup>-1</sup> at 0 MPa CO<sub>2</sub> to 1350 cm<sup>-1</sup> at 7 MPa CO<sub>2</sub>, and remained unchanged at 7–20 MPa CO<sub>2</sub>. The peak position of  $\nu_{as}(\text{NO}_2)$  was also blue shifted from 1521 to 1538 cm<sup>-1</sup> with CO<sub>2</sub> pressure up to ca. 5.5 MPa; between 5.5 and 20 MPa CO<sub>2</sub>, the peak position was slightly shifted to a lower wavenumber and then changed little. The absorption bands at 20 MPa CO<sub>2</sub> were located at larger wavenumbers than those at 0 MPa CO<sub>2</sub> and in ethanol. These FTIR results indicate that the N–O bond of the nitro group becomes stronger in the presence of dense phase CO<sub>2</sub> compared to the ambient gas and liquid conditions. Additionally, it was observed that an absorption band appeared at 1109 cm<sup>-1</sup> at 0 MPa CO<sub>2</sub> and was blue shifted to 1112 cm<sup>-1</sup> with CO<sub>2</sub> pressure up to 7 MPa, above which it did not change further (not shown). This band is due to the C–N stretch [43].

The above changes of  $\nu_s(\text{NO}_2)$  and  $\nu_{as}(\text{NO}_2)$  for *p*-CNB with CO<sub>2</sub> pressures were similar to those of nitrobenzene in dense phase CO<sub>2</sub> [37]. We have proposed that the

overall IR result of nitrobenzene in dense phase CO<sub>2</sub> is controlled by the following modes of interactions between CO<sub>2</sub> molecules and the nitro group: (1) one of the oxygen atoms of CO<sub>2</sub> interacts with the positive nitrogen of –NO<sub>2</sub> group, and (2) the carbon atom of CO<sub>2</sub> interacts with the oxygen of –NO<sub>2</sub> group. The former interaction might strengthen both the C–N and N–O bonds, while the latter might weaken the strength of the N–O bond. The former interaction has a dominant effect on the stretch vibration of N–O bond [37]. It seems likely that the nitro group of *p*-CNB interacts with CO<sub>2</sub> in the same modes as in the case of nitrobenzene.

At similar CO<sub>2</sub> pressures, the bands of  $\nu_s(\text{NO}_2)$  and  $\nu_{as}(\text{NO}_2)$  of *p*-CNB appeared at lower wavenumbers than those of the corresponding peaks of nitrobenzene. For example, the wavenumbers of  $\nu_s(\text{NO}_2)$  and  $\nu_{as}(\text{NO}_2)$  for *p*-CNB at 20 MPa CO<sub>2</sub> were 1350 and 1534 cm<sup>-1</sup>; the corresponding values for nitrobenzene were 1354 and 1538 cm<sup>-1</sup>, respectively [37]. The difference in wavenumbers of the nitro group vibrations between *p*-CNB and nitrobenzene might be due to the Cl substituent, an electron-withdrawing group attaching to the benzene ring of *p*-CNB.

### 3.4.2 *p*-CNSB

Fig. 7 shows the FTIR spectra of the nitroso (N=O) moiety of *p*-CNSB in the presence of 4 MPa H<sub>2</sub> and 0–20 MPa CO<sub>2</sub>. The spectrum of *p*-CNSB in ethanol at room

temperature was recorded for comparison. The absorption bands at 1109 and 1517  $\text{cm}^{-1}$  before the introduction of  $\text{CO}_2$  are due to the C–N stretch of the CNSB monomer and the stretching vibration of N=O, respectively [43]. The peak position of  $\nu(\text{C–N})$  of CNSB monomer was slightly blue shifted from 1109 to 1116  $\text{cm}^{-1}$  with the increase of  $\text{CO}_2$  pressure up to ca. 15 MPa and then remained unchanged. We have shown that the N=O group of nitrosobenzene can interact with  $\text{CO}_2$  molecules through its oxygen (O-interacted) and nitrogen (N-interacted) atoms; the stretching vibration of N=O gives a band around 1520  $\text{cm}^{-1}$  in the former case and a band at 1485  $\text{cm}^{-1}$  in the latter case [37]. Thus, the band at ca. 1510  $\text{cm}^{-1}$  in the spectra of *p*-CNSB would arise from the stretching vibration  $\nu(\text{N=O})(\text{O-interacted})$ . The peak position of  $\nu(\text{N=O})(\text{O-interacted})$  changed with  $\text{CO}_2$  pressure and these shifts are shown in Fig. 8. The stretching vibration  $\nu(\text{N=O})(\text{O-interacted})$  in  $\text{CO}_2$  was monotonously red shifted with  $\text{CO}_2$  pressure up to 13 MPa and then remained unchanged. Additionally, there was no peak at 1485  $\text{cm}^{-1}$  in the spectra of *p*-CNSB at all pressures examined. Therefore, the N=O of *p*-CNSB interacts with the carbon of  $\text{CO}_2$  through its oxygen but not through its nitrogen. The N=O group functions as a Lewis base (LB) and  $\text{CO}_2$  plays a role of a Lewis acid (LA). This type of intermolecular interaction becomes stronger with the increase in  $\text{CO}_2$  pressure and weakens the N=O bond of *p*-CNSB. Simultaneously, the C–N stretch band was blue

shifted, in agreement with previous results for nitroso compounds that  $\nu(\text{C-N})$  increases when  $\nu(\text{N=O})$  decreases [37, 43].

At 20 MPa  $\text{CO}_2$ , the peak position of  $\nu(\text{N=O})(\text{O-interacted})$  was at  $1506 \text{ cm}^{-1}$ , which was still higher than that in ethanol ( $1501 \text{ cm}^{-1}$ ). This difference is similar to that of nitrosobenzene, indicating the LA-LB interaction of  $\text{CO}_2$  with the  $\text{N=O}$  group of *p*-CNSB is also less strong compared with the hydrogen bonding in ethanol [37].

In the spectra of *p*-CNSB, the band of  $\nu(\text{N=O})(\text{O-interacted})$  was shifted from  $1517 \text{ cm}^{-1}$  at 0 MPa  $\text{CO}_2$  to  $1506 \text{ cm}^{-1}$  at 20 MPa  $\text{CO}_2$ ; in the case of nitrosobenzene, the same vibration gave a band at  $1521$  and  $1513 \text{ cm}^{-1}$  at the corresponding pressures [37]. That is, the stretching vibration of  $\text{N=O}$  of *p*-CNSB is less strong than that on nitrosobenzene at similar  $\text{CO}_2$  pressures. The difference might be due to the electron-withdrawing effect of the Cl substituent of *p*-CNSB.

### 3.4.3 *p*-CPHA

The FTIR spectra of *p*-CPHA in dense phase  $\text{CO}_2$  and in ethanol are given in Fig. 9. The absorption bands at ca.  $920$ ,  $1494\text{--}1500$ , and  $3200 \text{ cm}^{-1}$  are related to the  $\text{N-O}$  stretch, a ring stretching mode, and the  $\text{O-H}$  stretching vibration of phenylhydroxylamine derivatives, respectively [44, 45]. The  $\text{O-H}$  stretch band of *p*-CPHA in dense phase  $\text{CO}_2$  was not distinct at all pressures examined, possibly because  $\text{scCO}_2$  has a combination band in the region where the stretching vibration of  $\text{O-H}$  occurs [46]. The  $\text{N-O}$  stretch of *p*-CPHA could only be identified at  $915 \text{ cm}^{-1}$

above 8 MPa CO<sub>2</sub>, and its peak position did not show any shift with CO<sub>2</sub> pressures from 8 to 20 MPa. Here, our interest is focused on the absorption band at 1494 cm<sup>-1</sup>, which is related to the ring stretch of *p*-CPHA, for the discussion on interactions between *p*-CPHA and CO<sub>2</sub> molecules.

The position of the ring absorption band at 1494 cm<sup>-1</sup> scarcely changed between ca. 0 and 5 MPa CO<sub>2</sub>, and was blue shifted to 1498 cm<sup>-1</sup> with further increasing CO<sub>2</sub> pressure up to ca. 8 MPa. At 9.7–20.4 MPa CO<sub>2</sub>, the band split into two peaks at 1498 and 1505 cm<sup>-1</sup>, and their positions did not change with CO<sub>2</sub> pressures. The splitting of the ring absorption band was also observed for *N*-phenylhydroxylamine at above 8 MPa CO<sub>2</sub>; however, the band was red shifted at 4–11 MPa CO<sub>2</sub> and its position remained unchanged from 11 to 20 MPa CO<sub>2</sub> [37].

#### 3.4.4 CO<sub>2</sub>

Interactions of CO<sub>2</sub> with LB, polymer, or ionic liquids cause some changes in the IR spectra corresponding to the CO<sub>2</sub>  $\nu_2$ -bending (610–680 cm<sup>-1</sup>) and  $\nu_3$ -antisymmetric stretching (2100–2500 cm<sup>-1</sup>) mode regions [47-49]. It was impossible to distinguish the  $\nu_2$  mode in our IR results. Fig. 10 gives the FTIR spectra of CO<sub>2</sub> in the  $\nu_3$  region for the CO<sub>2</sub>-*p*-CNB, CO<sub>2</sub>-*p*-CNSB, and CO<sub>2</sub>-*p*-CPHA systems at different CO<sub>2</sub> pressures. The results in Fig. 10 were obtained by using the substrate-absent system at the corresponding pressures as background. For the CO<sub>2</sub>-*p*-CNB system, there was one

main peak at  $2347\text{ cm}^{-1}$  at  $\text{CO}_2$  pressures  $> 8\text{ MPa}$  and the peak position scarcely changed with  $\text{CO}_2$  pressure. For the  $\text{CO}_2$ -*p*-CNSB system, there was only one peak at  $2352\text{ cm}^{-1}$  at above  $9.5\text{ MPa}$ , and its position did not change with  $\text{CO}_2$  pressure. The fact that only one band appears in the  $\nu_3$  region suggests that there is only one type of the site within the *p*-CNB or *p*-CNSB molecule to interact with  $\text{CO}_2$  molecules [48].

Additionally, the wavenumber of the C=O stretching vibration of  $\text{CO}_2$  in the  $\text{CO}_2$ -*p*-CNB system was lower than that in the  $\text{CO}_2$ -*p*-CNSB system. This indicates that the C=O bond strength of  $\text{CO}_2$  is weaker in the  $\text{CO}_2$ -*p*-CNB system than that in the  $\text{CO}_2$ -*p*-CNSB system. The IR results of *p*-CNB have shown that the interaction of  $\text{CO}_2$  through its oxygen with the nitrogen of  $-\text{NO}_2$  group had a dominant effect on the stretching vibration of N–O bond; both the C–N and N–O bonds were strengthened. It seems likely that the interaction between  $\text{CO}_2$  and *p*-CNB induces partial electron transfer from the C=O bond of  $\text{CO}_2$  to the C–N and N–O bonds of *p*-CNB, and this weakens the C=O bond of  $\text{CO}_2$ . In contrast, the N=O of *p*-CNSB interacted with the carbon of  $\text{CO}_2$  through its oxygen (not nitrogen), and the N=O bond was weakened with  $\text{CO}_2$  pressures. The interaction of  $\text{CO}_2$  with *p*-CNSB is likely to induce partial electron transfer from the N=O bond of *p*-CNSB to the C=O bond of  $\text{CO}_2$ , strengthening the C=O bond. Thus, the IR spectra of  $\text{CO}_2$  provide additional evidence for the interaction

mode of CO<sub>2</sub> with *p*-CNB and *p*-CNSB.

Fig. 10(c) shows the FTIR difference spectra of CO<sub>2</sub> in the  $\nu_3$  region for the CO<sub>2</sub>-*p*-CPHA system at different pressures. At above 8.6 MPa CO<sub>2</sub>, there was one or two peaks at around 2351 cm<sup>-1</sup> with no other peaks in the  $\nu_3$  region. In contrast, an additional peak appears at 2332 cm<sup>-1</sup> along with the bands at 2348–2355 cm<sup>-1</sup> for the CO<sub>2</sub>-*N*-phenylhydroxylamine system [37]. This indicates that *p*-CPHA does interact with CO<sub>2</sub>; however, the available sites within the *p*-CPHA molecule for CO<sub>2</sub> are less than within the *N*-phenylhydroxylamine molecule. Presumably, CO<sub>2</sub> interacts with *p*-CPHA through its carbon.

### 3.5. Improvement of the selectivity to CAN

The dechlorination reaction was suppressed over Ni/TiO<sub>2</sub> in either ethanol or scCO<sub>2</sub>, which might be mainly related to the properties of Ni/TiO<sub>2</sub>. The formation of harmful intermediates occurring in ethanol was almost completely retarded in scCO<sub>2</sub>, indicating the significance of medium effects. The FTIR results show that the strength of the N–O bond of CNB in dense phase CO<sub>2</sub> was stronger than that in the ambient gas phase and it increased with CO<sub>2</sub> pressure up to ca. 6 MPa, above which it slightly decreased (Fig. 6). However, the strength of the N=O bond of CNSB was monotonously reduced with CO<sub>2</sub> pressure (Fig. 8). Namely, the reactivity of the –NO<sub>2</sub> group may

decrease with CO<sub>2</sub> pressure up to 6 MPa and will not change so much at higher pressures. In contrast, the reactivity of the N=O group may increase with CO<sub>2</sub> pressure. It is likely, therefore, that the hydrogenation of CNSB is more significantly accelerated than that of CNB when dense phase CO<sub>2</sub> is used. Moreover, the FTIR results indicate that interactions occurred between CPHA and dense phase CO<sub>2</sub> molecules. These interactions should promote the transformation of CPHA to CAN (step III in Scheme 1), contributing to the improved selectivity to CAN. As a result, CAN was formed with almost 100% selectivity in/under dense phase CO<sub>2</sub>. Therefore, the molecular interactions of CO<sub>2</sub> with the reacting species should be an important factor in determining the product selectivity over Ni/TiO<sub>2</sub>.

### **3.6. Reaction pathways for the hydrogenation of CNB in scCO<sub>2</sub> over Ni/TiO<sub>2</sub>**

The path IV in Scheme 1 occurs on Au/TiO<sub>2</sub>, and the step V becomes significant over Pd/Pt/Ni catalysts in the presence of vanadium promoters [2, 3, 7]. Herein, we discuss the reaction pathways over Ni/TiO<sub>2</sub> in dense phase CO<sub>2</sub> without the consideration of pathways IV and V. The total yield of all byproducts was <3.5% over the whole conversion range of 9–100% (Fig. 2 and Table 2). Accordingly, the condensation route (steps VI and VII) in Scheme 1 should be negligible, and the hydrogenation of CNB to CAN proceeds likely through the consecutive steps I→II→III.

The rate of CAN formation is determined by the slowest reaction rate among steps I, II, and III. The intermediates, detected by GC analysis, included CNSB and trace amounts of CAOB, CAB, and CHAB. These intermediates may be present in the reaction mixture; or they are absent in the reaction mixture but come from the decomposition of CPHA during the GC analysis [42]. Anyway, if the reaction rate of step II or III is the slowest, the amount of these intermediates should increase first and then decrease with the conversion of CNB. Fig. 2 shows that the yield of all byproducts decreased from 3.5% at 9% conversion to <1% at conversion >70%. The yield of CAN was similar to the conversion of CNB over the conversion range of 9–100%. In other words, the rate of CAN formation was almost equal to that of CNB conversion, i.e., the rate of step I. Therefore, in the present case of CNB hydrogenation in dense phase CO<sub>2</sub> over Ni/TiO<sub>2</sub>, the transformation of CNB to CNSB (step I in Scheme 1) seems to be the relatively slow step that determines the rate of CAN formation. The proposed reaction pathways may be related to the molecular interactions of CO<sub>2</sub> with CNB, CNSB, and CPHA. The relative reactivity of these reacting species was changed through interactions with CO<sub>2</sub> as discussed above, and consequently, the relative hydrogenation rates of steps I, II, and III are altered in dense phase CO<sub>2</sub>.

#### **4. Conclusions**

The chemoselective hydrogenation of CNB to CAN was achieved over Ni/TiO<sub>2</sub> in scCO<sub>2</sub> at 35°C. Both the accumulation of harmful intermediates and the formation of dechlorinated byproduct were suppressed effectively in scCO<sub>2</sub>. The selectivity to the desired product, CAN, was >97% over the conversion range of 9–100%. One of the important factors for this improved selectivity to CAN is the interactions of CO<sub>2</sub> with the reacting species, i.e., CNB, CNSB, and CPHA. The nitro group of CNB interacts with CO<sub>2</sub> through its nitrogen and oxygen atoms. The former mode has a dominant effect on the stretch vibration of N–O bond, and the reactivity of CNB is decreased. The nitroso group of CNSB interacts through its oxygen with the carbon of CO<sub>2</sub> and the reactivity of CNSB is increased. CPHA can also interact with scCO<sub>2</sub>, and the transformation of CPHA to CAN is likely promoted. Probably, the hydrogenation of CNB mainly occurs through the direct hydrogenation route, i.e., CNB→CNSB→CPHA→CAN. The transformation of CNB to CNSB might be the rate-determining step.

The strength of the N–O bond of CNB, the N=O bond of CNSB, and the N–O bond of CPHA is weaker compared with the corresponding bonds of nitrobenzene, nitrosobenzene, and *N*-phenylhydroxylamine, due to the electron-withdrawing effect of Cl substituent. There is no interaction between CO<sub>2</sub> and the nitrogen of N=O group of

CNSB, which is different from the modes of CO<sub>2</sub> interaction with nitrosobenzene. The available sites to interact with CO<sub>2</sub> are also less within the CPHA molecule than within the *N*-phenylhydroxylamine one.

### **Acknowledgments**

The authors gratefully acknowledge the financial support from the One Hundred Talent Program of CAS, NSFC 20873139, and KJCX2, YW.H16. This work was also supported by the Japan Society for the Promotion of Science with Grant-in-Aid for Scientific Research (B) 18360378 and by the CAS-JSPS international joint project GJHZ05. X. Meng thanks the Global COE (Center of Excellence) fellowship of Hokkaido University.

### **References**

- [1] X. Wang, M. Liang, J. Zhang, Y. Wang, *Curr. Org. Chem.* 11 (2007) 299.
- [2] A. Corma, P. Concepcion, P. Serna, *Angew. Chem., Int. Ed.* 46 (2007) 7266.
- [3] P. Baumeister, H.U. Blaser, M. Studer, *Catal. Lett.* 49 (1997) 219.
- [4] H.U. Blaser, A. Schnyder, H. Steiner, F. Rossler, P. Baumeister, in: G. Ertl, H. Knözinger, F. Schüth, J. Weitkamp (Eds.), *Handbook of Heterogeneous*

- Catalysis, Wiley-VCH Verlag GmbH & Co. KGaA, Weinheim, Germany, 2008,  
p. 3291.
- [5] F. Cardenas-Lizana, S. Gomez-Quero, M. Keane, *Appl. Catal. A* 334 (2008) 199.
- [6] A. Corma, P. Serna, *Science* 313 (2006) 332.
- [7] M. Studer, S. Neto, H.U. Blaser, *Top. Catal.* 13 (2000) 205.
- [8] N. Mahata, A.F. Cunha, J.J.M. Órfão, J.L. Figueiredo, *Catal. Commun.* 10 (2009) 1203.
- [9] F. Cárdenas-Lizana, S. Gómez-Quero, A. Hugon, L. Delannoy, C. Louis, M. Keane, *J. Catal.* 262 (2009) 235.
- [10] Y. Chen, C. Wang, H. Liu, J. Qiu, X. Bao, *Chem. Commun.* (2005) 5298.
- [11] Y. Chen, J. Qiu, X. Wang, J. Xiu, *J. Catal.* 242 (2006) 227.
- [12] D. He, H. Shi, Y. Wu, B. Xu, *Green Chem.* 9 (2007) 849.
- [13] L. Liu, B. Qiao, Y. Ma, J. Zhang, Y. Deng, *Dalton Trans.* (2008) 2542.
- [14] X. Wang, M. Liang, H. Liu, Y. Wang, *J. Mol. Catal. A* 273 (2007) 160.
- [15] M. Liang, X. Wang, H. Liu, H. Liu, Y. Wang, *J. Catal.* 255 (2008) 335.
- [16] F. Wang, J. Liu, X. Xu, *Chem. Commun.* (2008) 2040.
- [17] B. Coq, A. Tijani, R. Dutartre, F. Figuéras, *J. Mol. Catal.* 79 (1993) 253.
- [18] A. Corma, P. Serna, P. Concepción, J. Calvino, *J. Am. Chem. Soc.* 130 (2008)

8748.

- [19] J. Xiong, J. Chen, J. Zhang, *Catal. Commun.* 8 (2007) 345.
- [20] C. Xiao, H. Wang, X. Mu, Y. Kou, *J. Catal.* 250 (2007) 25.
- [21] C.A. Eckert, B.L. Knutson, P.G. Debenedetti, *Nature* 383 (1996) 313.
- [22] P.G. Jessop, W. Leitner, in: P.G. Jessop, W. Leitner (Eds.), *Chemical Synthesis Using Supercritical Fluids*, Wiley-VCH, Weinheim, Germany, 1999, p. 9.
- [23] A. Baiker, *Chem. Rev.* 99 (1999) 453.
- [24] B.M. Bhanage, M. Arai, *Catal. Rev.: Sci. Eng.* 43 (2001) 315.
- [25] J.R. Hyde, P. Licence, D. Carter, M. Poliakoff, *Appl. Catal. A* 222 (2001) 119.
- [26] W. Leitner, *Acc. Chem. Res.* 35 (2002) 746.
- [27] E.J. Beckman, *J. Supercrit. Fluid* 28 (2004) 121.
- [28] B. Subramaniam, M.A. McHugh, *Ind. Eng. Chem. Process Des. Dev.* 25 (1986) 1.
- [29] C.M. Rayner, *Org. Process Res. Dev.* 11 (2007) 121.
- [30] T. Seki, J.D. Grunwaldt, A. Baiker, *Ind. Eng. Chem. Res.* 47 (2008) 4561.
- [31] F. Zhao, S. Fujita, S. Akihara, M. Arai, *J. Phys. Chem. A* 109 (2005) 4419.
- [32] S. Ichikawa, M. Tada, Y. Iwasawa, T. Ikariya, *Chem. Commun.* (2005) 924.
- [33] F. Zhao, R. Zhang, M. Chatterjee, Y. Ikushima, M. Arai, *Adv. Synth. Catal.* 346

- (2004) 661.
- [34] F. Zhao, Y. Ikushima, M. Arai, *J. Catal.* 224 (2004) 479.
- [35] C. Xi, H. Cheng, J. Hao, S. Cai, F. Zhao, *J. Mol. Catal. A* 282 (2008) 80.
- [36] M. Mihaylov, E. Ivanova, Y. Hao, K. Hadjiivanov, H. Knözinger, B.C. Gates, *J. Phys. Chem. C* 112 (2008) 18973.
- [37] X. Meng, H. Cheng, Y. Akiyama, Y. Hao, W. Qiao, Y. Yu, F. Zhao, S. Fujita, M. Arai, *J. Catal.* 264 (2009) 1.
- [38] A. Defoin, *Synthesis* (2004) 706.
- [39] O. Kamm, C.S. Marvel, *Org. Synth.* 4 (1925) 57.
- [40] S. Ung, A. Falguières, A. Guy, C. Ferroud, *Tetrahedron Lett.* 46 (2005) 5913.
- [41] G. Bergeret, P. Gallezot, in: G. Ertl, H. Knözinger, F. Schüth, J. Weitkamp (Eds.), *Handbook of Heterogeneous Catalysis*, Wiley-VCH Verlag GmbH & Co. KGaA, Weinheim, Germany, 2008, p. 738.
- [42] S. Galvagno, A. Donato, G. Neri, R. Pietropaolo, Z. Poltarzewski, *J. Mol. Catal.* 42 (1987) 379.
- [43] S. Meijers, V. Ponc, *J. Catal.* 160 (1996) 1.
- [44] Y.K. Agrawal, *J. Chem. Eng. Data* 22 (1977) 70.
- [45] Y. Wu, J. Jiang, Y. Ozaki, *J. Phys. Chem. A* 106 (2002) 2422.

- [46] J.D. Grunwaldt, R. Wandeler, A. Baiker, *Catal. Rev.: Sci. Eng.* 45 (2003) 1.
- [47] T. Seki, J.D. Grunwaldt, A. Baiker, *J. Phys. Chem. B* 113 (2009) 114.
- [48] S.G. Kazarian, M.F. Vincent, F.V. Bright, C.L. Liotta, C.A. Eckert, *J. Am. Chem. Soc.* 118 (1996) 1729.
- [49] J.C. Dobrowolski, M.H. Jamróz, *J. Mol. Struct.* 275 (1992) 211.

### *Captions for Figures, Tables, and Scheme*

**Fig. 1.** (1) XRD patterns of Ni/TiO<sub>2</sub>: (a) calcined under air at 450°C, (b) reduced with H<sub>2</sub> at 450°C; (2) TEM image of Ni/TiO<sub>2</sub> after reduction with H<sub>2</sub> at 450°C.

**Fig. 2.** Evolution of species with time during the hydrogenation of *o*-CNB over 16 wt% Ni/TiO<sub>2</sub> in scCO<sub>2</sub> at 35°C. Reaction conditions: Ni/TiO<sub>2</sub> 0.15 g, CO<sub>2</sub> 11 MPa. (▲) *o*-CNB conversion, (○) *o*-CAN yield, (▽) total yield of all by-products.

**Fig. 3.** The phase behavior of *o*- (■, □), *m*- (▲, △) and *p*-CNB (▼, ▽) in CO<sub>2</sub> at 35°C in the presence of 4 MPa H<sub>2</sub>. A certain amount of *o*-CNB was added to the view cell, H<sub>2</sub> was introduced up to 4 MPa, and then CO<sub>2</sub> was gradually introduced until the liquid *o*-CNB disappeared at a CO<sub>2</sub> pressure P<sub>1</sub>. Upon carefully depressurization, the first liquid drop of *o*-CNB appeared at a pressure P<sub>2</sub>. These two pressures P<sub>1</sub> and P<sub>2</sub> were carefully determined at several amounts (concentrations in the cell) of *o*-CNB, and are given with solid and open marks, respectively. The data for *m*- and *p*-CNB were collected using the same procedures.

**Fig. 4.** Influence of CO<sub>2</sub> pressure on the conversion of *o*-CNB (●) and the selectivity to

*o*-CAN (○) in the hydrogenation of *o*-CNB over 16 wt% Ni/TiO<sub>2</sub> at 35°C and at H<sub>2</sub> 4 MPa for 50 min.

**Fig. 5.** FTIR spectra of nitro group stretching vibrations for *p*-CNB in the presence of 4 MPa H<sub>2</sub> and dense phase CO<sub>2</sub> at different pressures given. The spectra at CO<sub>2</sub> pressures <4 MPa and >5 MPa were collected at 90°C and 35°C, respectively. Also included are the same group vibrations of *p*-CNB in ethanol (*p*-CNB/ethanol = 0.05, molar ratio) at room temperature.

**Fig. 6.** Influence of CO<sub>2</sub> pressure on the absorption peak position of  $\nu_s(\text{NO}_2)$  and  $\nu_{as}(\text{NO}_2)$  of *p*-CNB. (○) Symmetric and (●) asymmetric stretching vibrations in dense phase CO<sub>2</sub>; (Δ) symmetric and (▲) asymmetric stretch in ethanol (*p*-CNB/ethanol = 0.05, molar ratio) at room temperature.

**Fig. 7.** FTIR spectra of *p*-CNSB in the presence of 4 MPa H<sub>2</sub> and dense phase CO<sub>2</sub> at pressures given. The spectra at CO<sub>2</sub> pressures <6 MPa and >6 MPa were collected at 90°C and 35°C, respectively. Also shown is the spectrum of *p*-CNSB in ethanol (*p*-CNSB /ethanol = 0.03, molar ratio) at room temperature.

**Fig. 8.** Influence of CO<sub>2</sub> pressure on the peak position of the nitroso group

(O-interacted) vibration for *p*-CNSB at 35°C. The spectrum in the absence of CO<sub>2</sub> (0 MPa) was collected at 90°C. Also shown is the same group vibration in ethanol (*p*-CNSB/ethanol = 0.03, molar ratio) at room temperature.

**Fig. 9.** FTIR spectra for the ring stretching vibration of *p*-CPHA in the presence of 4

MPa H<sub>2</sub> and dense phase CO<sub>2</sub> at pressures given (35°C). The spectrum of *p*-CPHA in ethanol (*p*-CPHA/ethanol = 0.15, molar ratio) collected at room temperature is also shown.

**Fig. 10.** FTIR difference spectra in the CO<sub>2</sub> ν<sub>3</sub>-antisymmetric-stretching mode region

for the CO<sub>2</sub>-*p*-CNB (a), CO<sub>2</sub>-*p*-CNSB (b), and CO<sub>2</sub>-CPHA (c) system at CO<sub>2</sub> pressures given. All spectra were collected at 35°C in the presence of 4 MPa H<sub>2</sub>. The difference spectra were obtained by using the substrate-absent system at the corresponding pressures as background.

**Table 1** Hydrogenation of *o*-CNB over 41 wt% Ni/Al<sub>2</sub>O<sub>3</sub> in scCO<sub>2</sub> and over 16 wt%

Ni/TiO<sub>2</sub> in different reaction media.

**Table 2** Results of hydrogenation of *m*- and *p*-CNB in scCO<sub>2</sub> over 16 wt% Ni/TiO<sub>2</sub>.

**Scheme 1** Possible reaction pathways for the hydrogenation of CNB to CAN [2–5].

CNB: Chloronitrobenzene, CNSB: chloronitrosobenzene, CPHA:

*N*-chlorophenylhydroxylamine, CAN: chloroaniline, CAOB: dichloroazoxybenzene,

CAB: dichloroazobenzene, CHAB: dichlorohydrazobenzene, AN: aniline.

*Tables, Figures, and Scheme*

**Table 1** Hydrogenation of *o*-CNB over 41 wt% Ni/Al<sub>2</sub>O<sub>3</sub> in scCO<sub>2</sub> and over 16 wt% Ni/TiO<sub>2</sub> in different reaction media.

Entry	Medium	Catalyst	C <sub>0</sub> <sup>a</sup> (mmol cm <sup>-3</sup> )	Conv. (%)	Selectivity (%)			TOF <sup>b</sup> (h <sup>-1</sup> )
					<i>o</i> -CAN	AN	Others	
1	scCO <sub>2</sub>	Ni/Al <sub>2</sub> O <sub>3</sub>	0.19	78 <sup>c</sup>	>98	<1.5	<0.5	90
2	scCO <sub>2</sub>	Ni/TiO <sub>2</sub>	0.19	82	99	<1	<1	318
3	Ethanol <sup>d</sup>	Ni/TiO <sub>2</sub>	0.19	26	70	<1	>29 <sup>e</sup>	101
4	Ethanol	Ni/TiO <sub>2</sub>	0.95	36	70	— <sup>f</sup>	30 <sup>e</sup>	140
5	<i>n</i> -Hexane	Ni/TiO <sub>2</sub>	0.95	59	97	2	1	229

Reaction conditions: H<sub>2</sub> 4 MPa, *o*-CNB 1.5 g (9.52 mmol), Ni/Al<sub>2</sub>O<sub>3</sub> 0.1 g or Ni/TiO<sub>2</sub> 0.15 g, organic solvent 10 cm<sup>3</sup> or CO<sub>2</sub> 10.5 MPa, reactor 50 cm<sup>3</sup>, 35°C, 50 min.

<sup>a</sup> Initial concentration of *o*-CNB.

<sup>b</sup> Turnover frequency of hydrogenation of *o*-CNB. The number of active sites was calculated using the average nickel diameter (*d*) determined by XRD line broadening via the following equation: Dispersion = 6(*v<sub>m</sub>* / *a<sub>m</sub>*) / *d*, where *v<sub>m</sub>* and *a<sub>m</sub>* are equal to 10.95 Å<sup>3</sup> and 6.51 Å<sup>2</sup>, respectively, for Ni [41].

<sup>c</sup> After 60 min of reaction.

<sup>d</sup> Ethanol 50 cm<sup>3</sup>, reactor 100 cm<sup>3</sup>.

<sup>e</sup> Other products in ethanol include CNSB, CAOB, CAB, and CHAB.

<sup>f</sup> Not detected.

**Table 2** Results of hydrogenation of *m*- and *p*-CNB in scCO<sub>2</sub> over 16 wt% Ni/TiO<sub>2</sub>.

Entry	Reactant	CO <sub>2</sub> (MPa)	Time (min)	Conv. (%)	Selectivity (%)		
					CAN	AN	Others
1	<i>m</i> -CNB	11	30	64	96	<0.1	4
2			80	100	>99.5	<0.5	<0.1
3	<i>p</i> -CNB	10	30	51	99	— <sup>a</sup>	1
4			90	100	>97	<0.5	<2.5

Reaction conditions: CNB 1.5 g (9.52 mmol), H<sub>2</sub> 4 MPa, 16 wt% Ni/TiO<sub>2</sub> 0.15 g, 35°C.

<sup>a</sup> Not detected.

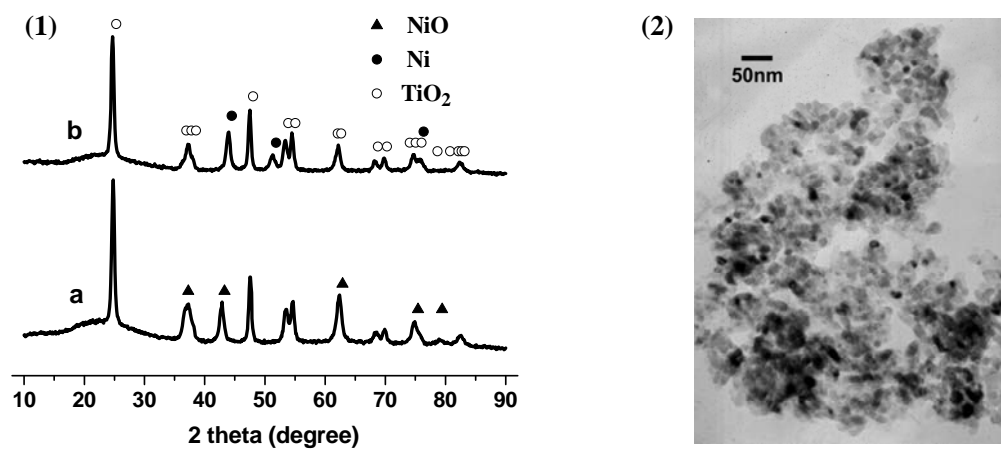


**Fig. 1.** (1) XRD patterns of Ni/TiO<sub>2</sub>: (a) calcined under air at 450°C, (b) reduced with H<sub>2</sub> at 450°C; (2) TEM image of Ni/TiO<sub>2</sub> after reduction with H<sub>2</sub> at 450°C.

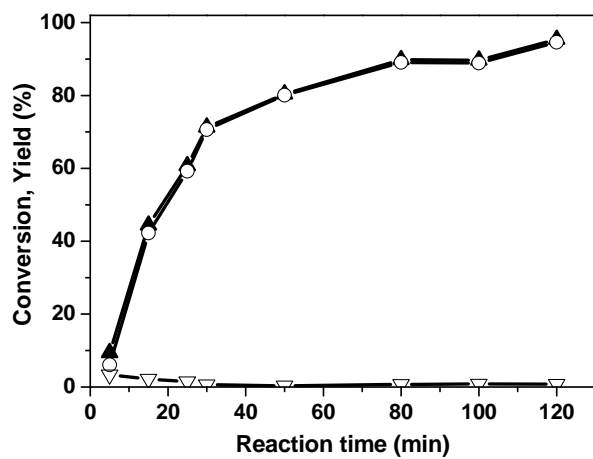


**Fig. 2.** Evolution of species with time during the hydrogenation of *o*-CNB over 16 wt% Ni/TiO<sub>2</sub> in scCO<sub>2</sub> at 35°C. Reaction conditions: Ni/TiO<sub>2</sub> 0.15 g, CO<sub>2</sub> 11 MPa. (▲) *o*-CNB conversion, (○) *o*-CAN yield, (▽) total yield of all by-products.

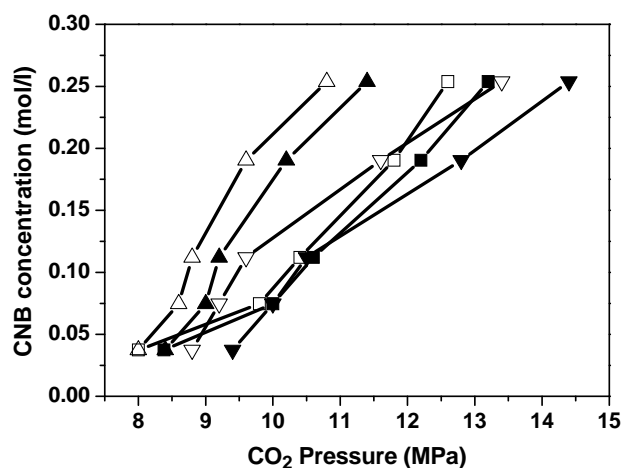


**Fig. 3.** The phase behavior of *o*- (■, □), *m*- (▲, △) and *p*-CNB (▼, ▽) in CO<sub>2</sub> at 35°C in the presence of 4 MPa H<sub>2</sub>. A certain amount of *o*-CNB was added to the view cell, H<sub>2</sub> was introduced up to 4 MPa, and then CO<sub>2</sub> was gradually introduced until the liquid *o*-CNB disappeared at a CO<sub>2</sub> pressure P<sub>1</sub>. Upon carefully depressurization, the first liquid drop of *o*-CNB appeared at a pressure P<sub>2</sub>. These two pressures P<sub>1</sub> and P<sub>2</sub> were carefully determined at several amounts (concentrations in the cell) of *o*-CNB, and are given with solid and open marks, respectively. The data for *m*- and *p*-CNB were collected using the same procedure.

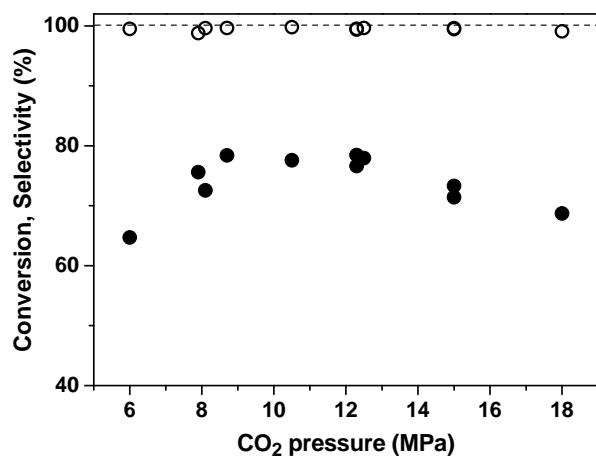


**Fig. 4.** Influence of CO<sub>2</sub> pressure on the conversion of *o*-CNB (●) and the selectivity to *o*-CAN (○) in the hydrogenation of *o*-CNB over 16 wt% Ni/TiO<sub>2</sub> at 35°C and at H<sub>2</sub> 4 MPa for 50 min.

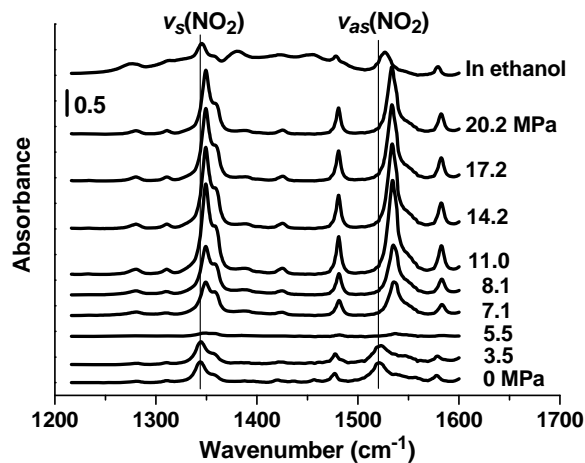


**Fig. 5.** FTIR spectra of nitro group stretching vibrations for *p*-CNB in the presence of 4 MPa H<sub>2</sub> and dense phase CO<sub>2</sub> at different pressures given. The spectra at CO<sub>2</sub> pressures <4 MPa and >5 MPa were collected at 90°C and 35°C, respectively. Also included are the same group vibrations of *p*-CNB in ethanol (*p*-CNB/ethanol = 0.05, molar ratio) at room temperature.

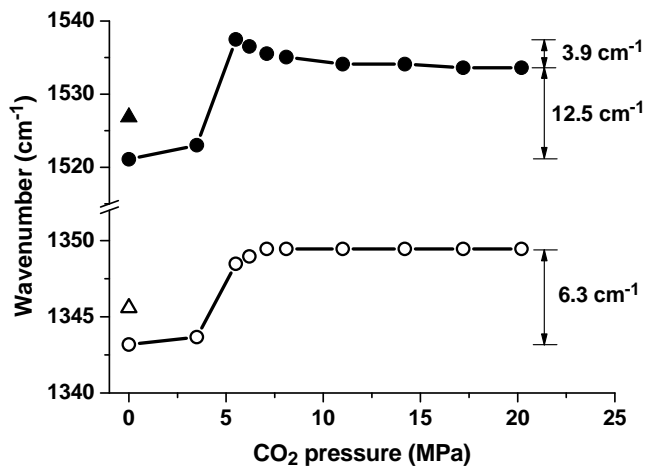


**Fig. 6.** Influence of CO<sub>2</sub> pressure on the absorption peak position of  $\nu_s(\text{NO}_2)$  and  $\nu_{as}(\text{NO}_2)$  of *p*-CNB. (○) Symmetric and (●) asymmetric stretching vibrations in dense phase CO<sub>2</sub>; (Δ) symmetric and (▲) asymmetric stretch in ethanol (*p*-CNB/ethanol = 0.05, molar ratio) at room temperature.

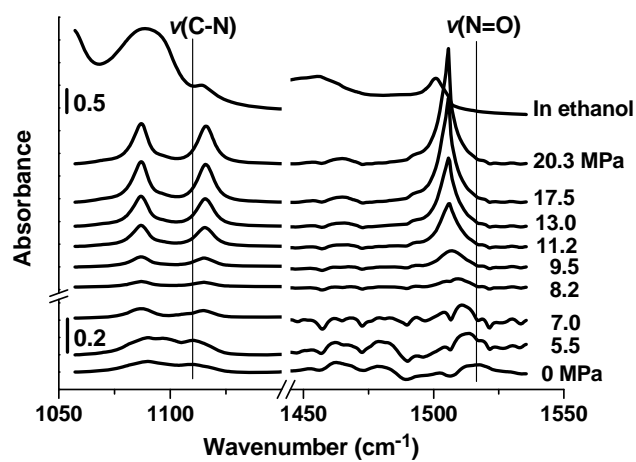


**Fig. 7.** FTIR spectra of *p*-CNSB in the presence of 4 MPa H<sub>2</sub> and dense phase CO<sub>2</sub> at pressures given. The spectra at CO<sub>2</sub> pressures <6 MPa and >6 MPa were collected at 90°C and 35°C, respectively. Also shown is the spectrum of *p*-CNSB in ethanol (*p*-CNSB /ethanol = 0.03, molar ratio) at room temperature.

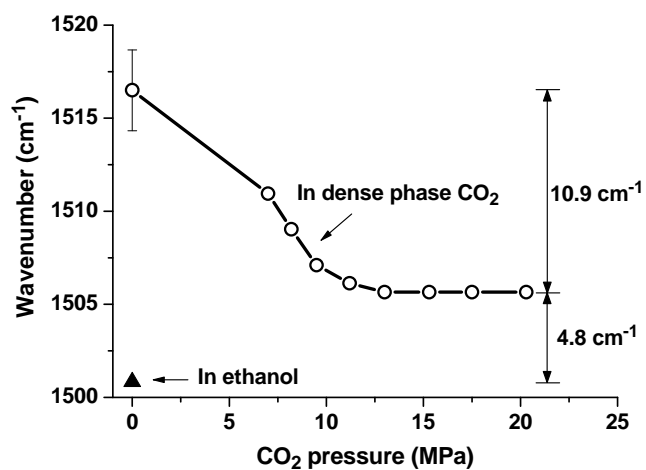
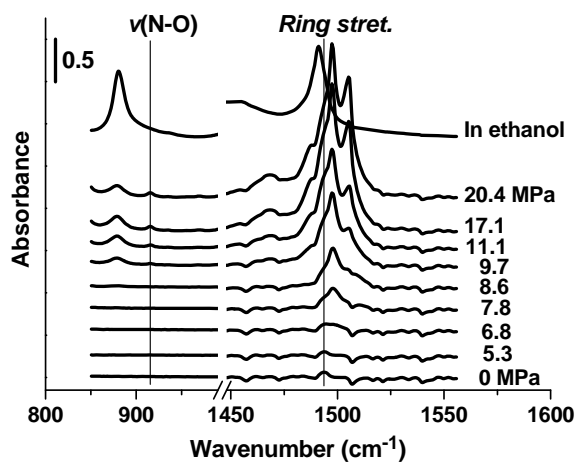


**Fig. 8.** Influence of CO<sub>2</sub> pressure on the peak position of the nitroso group

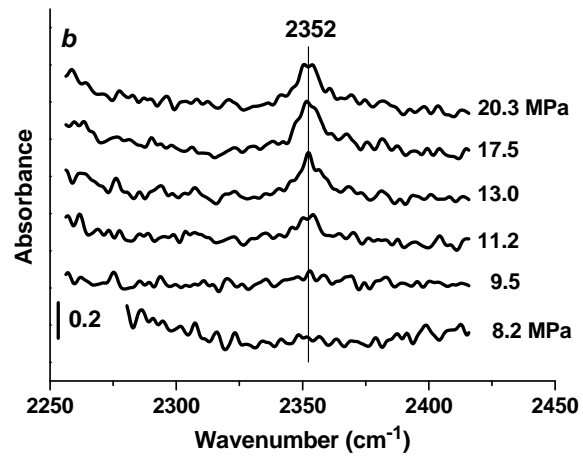
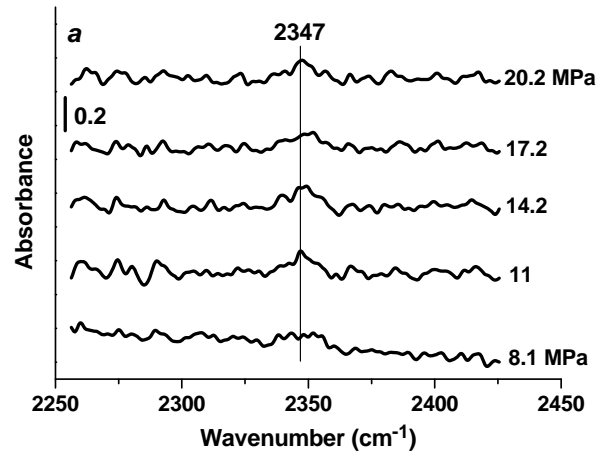
(O-interacted) vibration for *p*-CNSB at 35°C. The spectrum in the absence of CO<sub>2</sub> (0

MPa) was collected at 90°C. Also shown is the same group vibration in ethanol

(*p*-CNSB/ethanol = 0.03, molar ratio) at room temperature.



**Fig. 9.** FTIR spectra for the ring stretching vibration of *p*-CPHA in the presence of 4 MPa H<sub>2</sub> and dense phase CO<sub>2</sub> at pressures given (35°C). The spectrum of *p*-CPHA in ethanol (*p*-CPHA/ethanol = 0.15, molar ratio) collected at room temperature is also shown.



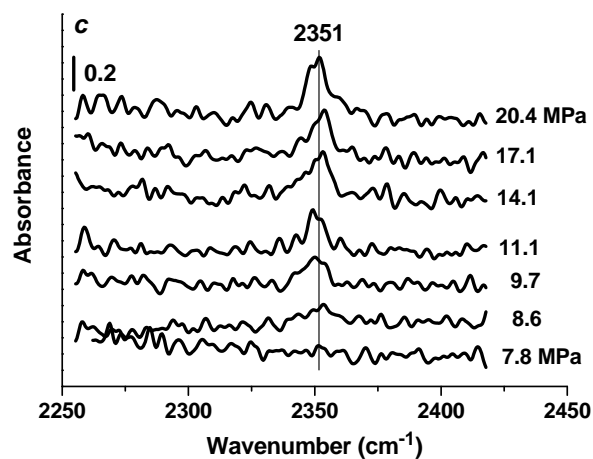
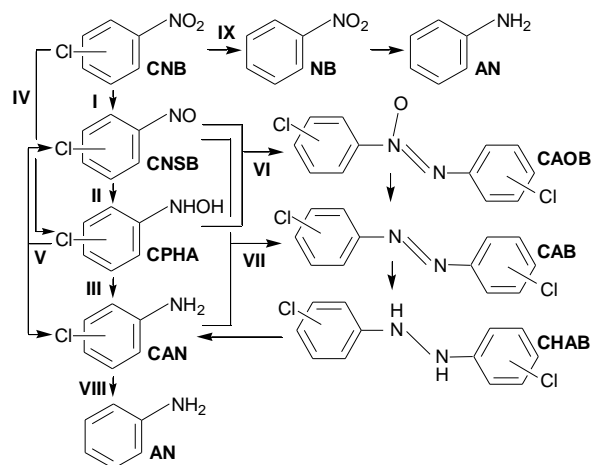


**Fig. 10.** FTIR difference spectra in the CO<sub>2</sub>  $\nu_3$ -antisymmetric-stretching mode region for the CO<sub>2</sub>-*p*-CNB (a), CO<sub>2</sub>-*p*-CNSB (b), and CO<sub>2</sub>-CPHA (c) system at CO<sub>2</sub> pressures given. All spectra were collected at 35°C in the presence of 4 MPa H<sub>2</sub>. The difference spectra were obtained by using the substrate-absent system at the corresponding pressures as background.



**Scheme 1** Possible reaction pathways for the hydrogenation of CNB to CAN [2–5].

CNB: Chloronitrobenzene, CNSB: chloronitrosobenzene, CPHA:

*N*-chlorophenylhydroxylamine, CAN: chloroaniline, CAOB: dichloroazoxybenzene,

CAB: dichloroazobenzene, CHAB: dichlorohydrazobenzene, AN: aniline.